A Novel Synthetic Route For Cerium Nickel Mixed Oxide ($CeNi_{0.5}O_y$) Nanoparticles And Study Of Its Hydrogen Storage Property

P.J. Elsa, C.B. Jeena, P.P. Moly, K.J. Ambily

Abstract - Cerium nickel mixed oxide nanoparticles ($CeNi_{0.5}O_y$) were synthesized by a novel method involving co-precipitation of nickel dimethyl glyoxime and ceric hydroxide from a solution of ammonium cerium nitrate [$(NH_4)_2Ce(NO_3)_4$] and nickel nitrate [$Ni(NO_3)_2$] using dimethyl glyoxime and ammonium hydroxide as precipitating agents. The dried powder was then converted to mixed oxide ($CeNi_{0.5}O_y$) by calcination in air at 500 °C for 2 hours. The calcined powder was characterized by X-ray Diffraction (XRD), FT-IR spectroscopy, UV-Vis absorption spectroscopy and Fluorescence spectroscopy. From the XRD data, the average primary crystallite size was found to be 4-5 nm. On heating with oxalic acid at 400 ºC for 30 min, the $CeNi_{0.5}O_y$ powder was found to be partially reduced as evident from XRD data. The hydrogen insertion properties of the $CeNi_{0.5}O_y$ were studied by temperature-programmed reduction method (TPR), and maximum hydrogen of 22.46 mLg^{-1} (20 wt %) was found to be inserted at 468.6 ºC.

Index Terms: $CeNi_{0.5}O_y$ mixed oxide nanoparticles, Co-precipitation, Oxalic acid, Hydrogen insertion, TPR

1 INTRODUCTION

Since nanostructured cerium oxide possess superior material properties for a variety of applications such as three-way catalysis for automobiles, production of hydrogen [1], oxygen sensors [2], as electrolytes in solid oxide fuel cells [3] etc, synthesis of such materials have attracted considerable attention recently. Cerium oxide adopts fluorite structure and may exist in two stable oxidation states, Ce^{3+} and Ce^{4+} [3]. The facile conversion between these two oxidation states may lead to oxygen storage/release capacity under oxidizing conditions and reducing conditions, respectively. As a consequence, cerium oxide can exist over a range of possible stoichiometries. By doping ceria with a second metal, it is possible to change the energetics for the Ce^{3+} and Ce^{4+} conversion [4]. Hence the properties of the ceria can be tuned by optimum doping with other metals for making materials with desired properties.

The deviation of stochiometry under reducing atmosphere from the ideal CeO_2 composition has also been studied by several temperature-programmed reductions (TPR) with hydrogen as the reductant. These studies have given rise to a substantial controversy about whether hydrogen atoms are merely chemisorbed on the CeO_2 surface or whether they enter the bulk of the crystal. Based on DFT calculations Karl Sohlberg et al. [5] have concluded that the uptake of small amounts of hydrogen leads to the formation of hydroxyl groups within the bulk of the crystals and also slightly expand the lattice. Their predicted hydrogen content, OH vibrational frequency, and ceria lattice expansion after hydrogen uptake were consistent with available experimental data. The redox properties of the ceria can also change with the size of the particles. In the case of bulk cerium oxide, only surface oxygen atoms are involved in the redox processes whereas in nanostructured ceria both surface and bulk oxygen atoms are involved. The preparation of ceria in the nanostructured form will lead to many attractive properties, such as high surface area, tunable pore size and surface chemistry, abundant surface defects and may significantly enhance their potential applications in various fields such as catalysis.

Presence of noble metals like Pt, Pd and Rh as well as transition metals like Ni and Cu improve the activity and selectivity of ceria catalyst for hydrogenation reaction [1]. Hence much efforts have been focused in the recent years on the synthesis of nanostructured intermetallic compounds of cerium oxide because of their promising applications in fuel cells [6], hydrogen storage materials [7], catalysts for hydrogenation reactions [8], CO and hydrocarbon oxidation and water- gas shift reactions [9]. Presence of nickel in Ni/Ce mixed oxides allows the adsorption of hydrogen followed by dissociation into atoms and migration to support during hydrogenation reactions [1].

Several methods, such as co-precipitation, impregnation, sol-gel method has been used for the synthesis of $CeNi_{0.5}O_y$mixed oxide nanopowders [10] among which the co-precipitation method is a simple process which ensures thorough mixing between cerium and the transition elements on an atomic level [11]. In this work, we report a novel method for the synthesis of $CeNi_{0.5}O_y$ mixed oxide nanoparticles (where Ni/Ce atomic ratio is 0.5), using dimethyl glyoxime and ammonium hydroxide as precipitating agents. The structural properties of $CeNi_{0.5}O_y$ mixed oxide nanoparticles were studied by X-ray diffraction (XRD), FT-IR spectroscopy, UV-Vis spectroscopy, SEM, Raman spectroscopy and Fluorescence spectroscopy.

Reduction of ceria based oxides under hydrogen atmosphere have been extensively studied [1], [4], [9], [12]. As an alternate for pure hydrogen, thermal decomposition of oxalic acid is an efficient and safe method for generating a reducing atmosphere for reduction reactions [13]. A simple method for the reduction of $CeNi_{0.5}O_y$ mixed oxide, employing thermal decomposition of oxalic acid at high temperature is also reported in the present work. A possible mechanism for the insertion of hydrogen in to the fluorite lattice of $CeNi_{0.5}O_y$ during the reduction is proposed.

2. EXPERIMENTAL

2.1. Synthesis of $CeNi_{0.5}O_y$ mixed oxide nanoparticles

All reagents are of analytical purity and were received from Sigma Aldrich. 10 g ammonium cerium nitrate $[(NH_4)_2Ce(NO_3)_4]$ and 2.65 g nickel nitrate hexahydrate $[(Ni(NO_3)_2.6H_2O)]$ were dissolved in a minimum amount of deionized water. Then a solution of 1.5 g dimethyl glyoxime (DMG) in 75 ml ethanol was added, followed by excess ammonium hydroxide (NH_4OH). The mixed precipitate of nickel dimethyl glyoxime and ceric hydroxide thus formed was filtered, washed with de-ionized water, dried at 100 ºC and finally calcined at 500 ºC for 2h to obtain $CeNi_{0.5}O_y$ nanoparticles.

2.2. Reduction of $CeNi_{0.5}O_y$ mixed oxide nanoparticles with oxalic acid

0.5 g $CeNi_{0.5}O_y$ nanopowder was mixed well with 5 g oxalic acid and crucible containing the sample was kept in a closed stainless steel vessel and heated at 400 ºC for 30 min in a muffle furnace. The thermal decomposition of oxalic acid causes partial reduction of $CeNi_{0.5}O_y$ nanoparticles.

2.3. Structural characterization

Crystal structure of the synthesized samples was investigated by XRD technique using X-ray Powder diffractometer (Bruker AXS D8 Advance) with Cu-Kα radiation (λ=0.15406 nm) as an X-ray source. The XRD patterns were recorded in the 2θ range 10-90° with a scan rate of 0.03°/min. The average crystallite size (D) of the mixed oxide was calculated by the Debye-Scherrer equation:

$$D = K\lambda/\beta_{2\theta}\cos\theta$$

where K is the shape factor, λ is the X-ray wavelength, β is the line broadening at half the maximum intensity (FWHM) in radians and θ is the Bragg's angle.

FT-IR spectra of $CeNi_{0.5}O_y$ mixed oxide were recorded in the wavenumber range from 400-4000 cm-1 by ThermoNicolet, Avatar-370 FT-IR Spectrometer. UV–Vis absorption spectra were recorded at room temperature on a Perkin Elmer spectrophotometer. The fluorescence spectral measurements were performed on a JASCO spectrofluorometer. FT-Raman spectra of the samples were recorded with a BRUKER RFS 27: Standalone FT-Raman Spectrometer. The TPR analysis was carried out using Temperature Programmed Desorption/Reduction/ Oxidation analyser.

3. RESULTS AND DISCUSSION

3.1.1. XRD analysis of $CeNi_{0.5}O_y$

Fig. 1(a) shows the XRD pattern of the synthesized $CeNi_{0.5}O_y$ powder. The peaks observed at 28.33, 32.77, 47.41, 56.18 corresponds to (111), (200), (220), (311) crystal planes of CeO_2 phase (JCPDS file 34-0394) and peaks at 43.19, 62.5, 75.6 are corresponds to (002), (022), (113) crystal planes of NiO phase (JCPDS file 4-0835)[14] and the solid have a typical cubic fluorite structure [8]. The average crystallite size calculated using Debye-Scherrer formula was found to be 4-5 nm.

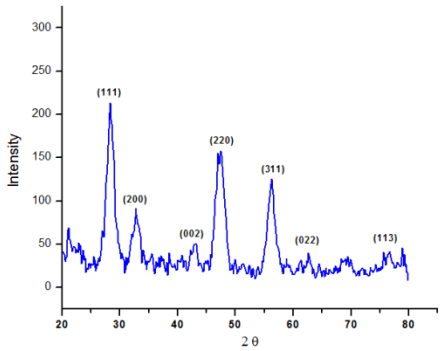

Fig.1: XRD pattern of $CeNi_{0.5}O_y$

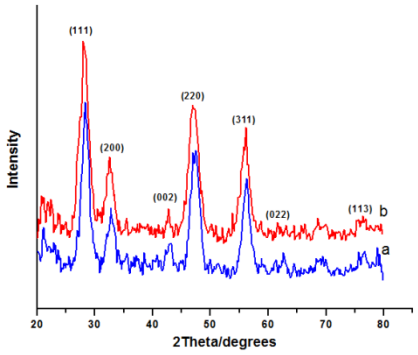

Fig.2: XRD pattern of $CeNi_{0.5}O_y$ (a) and reduced $CeNi_{0.5}O_y$ (b)

The XRD pattern of $CeNi_{0.5}O_y$ after reduction with oxalic acid is shown in Fig.1(b), in which peaks corresponding to (111), (220), (311) and (002) planes of $CeNi_{0.5}O_y$ were shifted towards lower angles. The shifts in the Bragg's angle of $CeNi_{0.5}O_y$ after reduction is presented in Table 1. The shift is approximately of 0.4º for reflections from most of the crystal planes. The shifting is attributed to the lattice expansion by the formation of anionic vacancies and the insertion of hydrogen into the lattice [8].

Table1-Bragg's angle of $CeNi_{0.5}O_y$ before and after reduction

Crystal planes	$CeNi_{0.5}O_y$ (2θ)	Reduced $CeNi_{0.5}O_y$ (2θ)
(111)	28.33 º	27.96 º
(002)	43.19 º	42.80 º
(220)	47.41 º	46.99 º
(311)	56.18 º	56.13 º

Since the reduction of Ni^{2+} in $CeNi_{0.5}O_y$ is much easier than the Ce^{4+} reduction, the presence of Ni^{2+} ions contributes to the creation of more anionic vacancies at lower temperatures. This makes hydrogen insertion easier in $CeNi_{0.5}O_y$, which leads to the expansion of the lattice to a greater extent than pure CeO_2 [8]. Oxalic acid was thermally decomposed at 400 ºC to yield a mixture of hydrogen, carbon monoxide and carbon dioxide and thus provide a reducing atmosphere [15].

Carpentier et al. [12] reported that during reduction, the anionic vacancies in the lattice of $CeNi_{0.5}O_y$ receive hydrogen in a hydride form created by the heterolytic splitting of H_2. In the present study, we propose a mechanism for the insertion of hydrogen into the fluorite lattice of $CeNi_{0.5}O_y$ as follows:

$$O^{2-}\ Mn^{+}\ [A]^{+}\ H_2 \rightarrow OH^{-}\ Mn^{+}\ H^{-}$$

where [A] is the anionic vacancy [12]. Considering the relative size of H^-, OH^- and O^{2-} (1.54, 1.76 and 1.32 Å, respectively), the lattice expansion observed in the reduction step corresponds to the substitution of O^{2-} species by an H^- and OH^- species [9].

3.2. FT-IR Analysis

Fig 2(a) shows the FT-IR spectrum of the synthesized $CeNi_{0.5}O_y$ powder. The broad weak band at 3375 cm^{-1} is assigned to the stretching vibration and bands at 1641, 1504, 1359 are due to the bending vibrations of surface hydroxyl groups of ceria [16]. The broad band below 450 cm^{-1} is attributed to the characteristic stretching vibrations of Ce-O and Ni-O bonds [17].

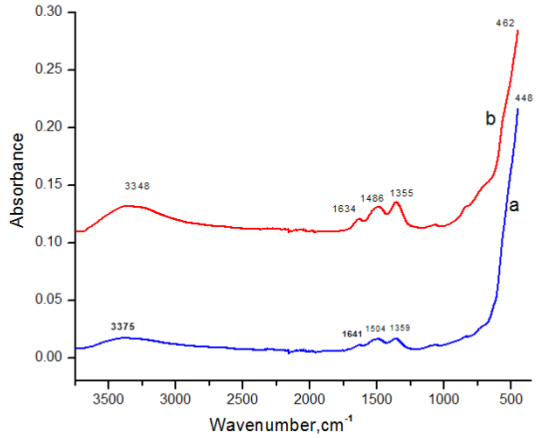

Fig.3: FT-IR spectra of $CeNi_{0.5}O_y$ (a) and reduced $CeNi_{0.5}O_y$ (b).

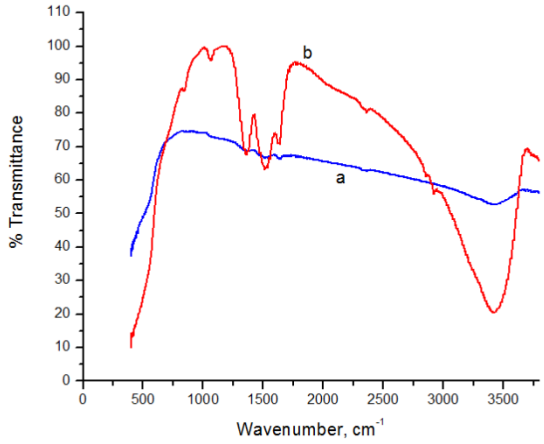

Fig.4: Transmittance spectra of $CeNi_{0.5}O_y$ (a) and reduced $CeNi_{0.5}O_y$ (b).

3.3. UV-Vis absorption spectroscopy

The UV–Vis absorption spectra of prepared $CeNi_{0.5}O_y$ nanoparticles are shown in Figure 5. For CeO_2 nanoparticles, the strong absorption band at 380 nm corresponds to a band gap energy of 3.26 eV. However, in $CeNi_{0.5}O_y$ the band shifted towards the lower wavelength side of 310 nm, which shows the blue shift. It indicates the formation of $CeNi_{0.5}O_y$. [18].

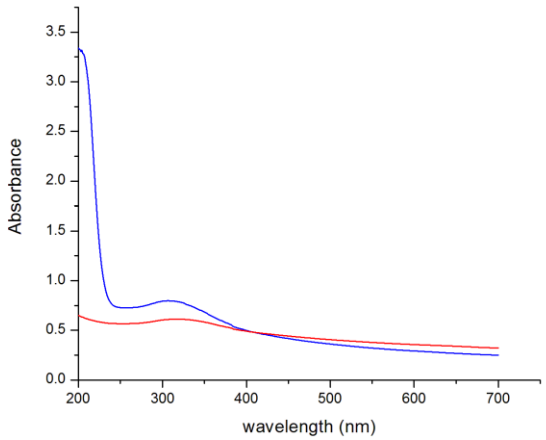

Fig.5: UV-Vis spectrum of (a) $CeNi_{0.5}O_y$ (blue line) (b) reduced $CeNi_{0.5}O_y$ (red line)

3.4. Fluorescence spectroscopy

Figure 6 shows the fluorescence spectrum of $CeNi_{0.5}O_y$ with excited wavelength of 300 nm. The prepared $CeNi_{0.5}O_y$ have emission bands at 318 nm, 344 nm, 414 nm, 436 nm,468 nm and small bands at 482 nm and 491 nm. CeO2 nanorods have three emission peaks located at 370, 414 and 468 nm [19].The PL spectrum of CeO_2 nanoparticles shows emission bands at 322 nm, 425 nm due to the presence of defects and two weak emission bands around at 460 and 480 nm due to oxygen vacancies. [20]. The pure NiO nanoparticles show emission bands at 364 nm, 439, 481 nm and 527 nm, respectively [18].

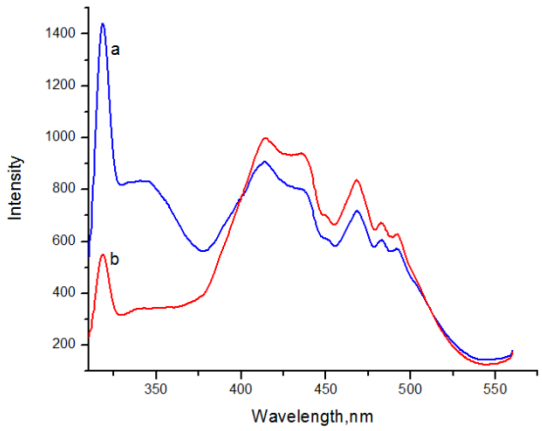

Fig.6: Emission spectrum of $CeNi_{0.5}O_y$ (blue line) (a) and reduced $CeNi_{0.5}O_y$ (red line) (b).

3.5. Raman spectroscopy

Figure 7 shows the Raman spectrum of $CeNi_{0.5}O_y$. The CeO_2 and ceria-doped materials show a band at around 465 cm^{-1} of F_{2g} mode, due to the symmetric stretching of Ce-O vibrational unit of CeO_2 [21]. It shifts to lower frequency of 443.74 cm^{-1} in Ce–Ni mixed oxides [22].

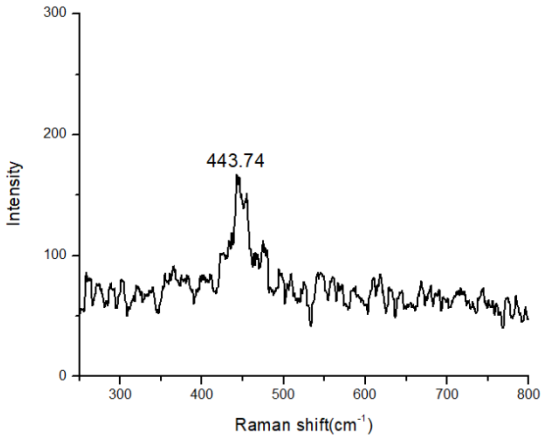

Fig.7: Raman spectrum of $CeNi_{0.5}O_y$.

3.6. SEM Analysis

Figure 8 shows the SEM image of $CeNi_{0.5}O_y$. From the morphology, we can see the porous nature of the nanomaterial surface, which is suitable for hydrogen adsorption.

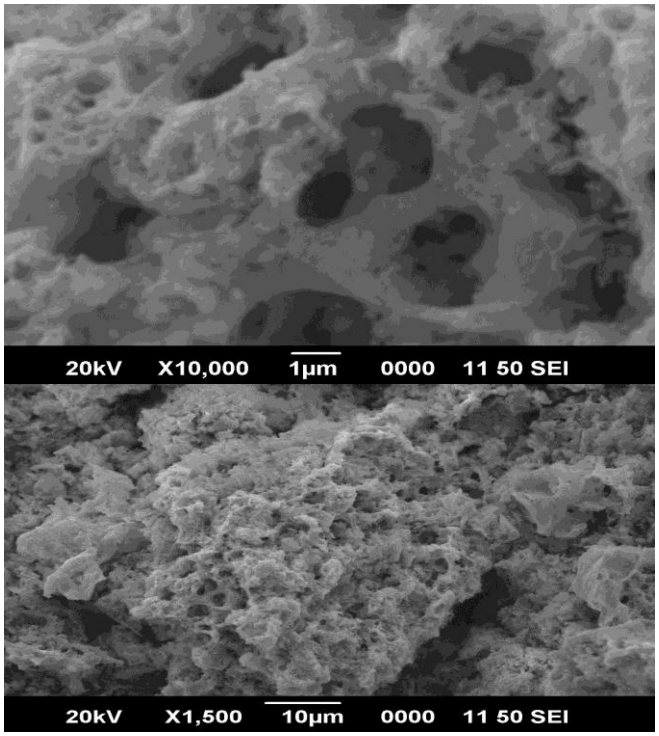

Fig.8: SEM images of $CeNi_{0.5}O_y$.

3.7. TPR Analysis (Temperature Programmed Reduction)

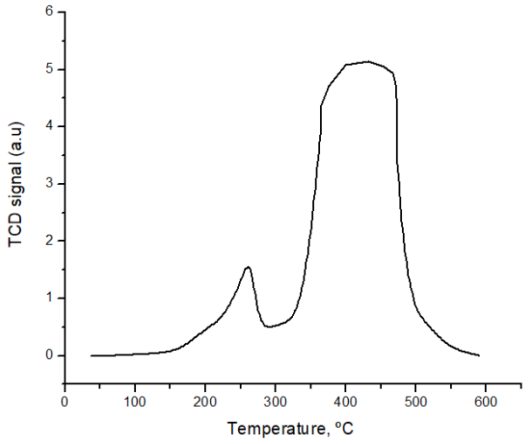

Fig.9: TPR spectra of H_2 adsorbed on $CeNi_{0.5}O_y$.

The total hydrogen consumed during Temperature Programmed Reduction of the sample is reported in table 2.

Table 2 - TPR peaks and global H_2 consumed.

TPR peaks (°C)	H_2 cons. (mLg−1)	H_2 cons. (10−3 mol g−1)	H_2 cons. (wt%)
249.3	0.83066	0.0370	0.74
260.2	4.48813	0.2002	4.004
468.6	22.46559	1.0023	20.046
668.5	0.24409	0.0108	0.216
674.9	0.45536	0.0203	0.406

A maximum of 22.46 mL/g at STP of hydrogen intake was observed at 468.6°C. The small peak appeared at 260.2°C, was attributed to the easy reduction of oxygen adsorbed on the vacancies of the catalysts [23]. The TPR results strongly support hydrogen adsorption nature of $CeNi_{0.5}O_y$.

4. Conclusion

Cerium nickel mixed oxide nanoparticles ($CeNi_{0.5}O_y$) were successfully synthesized by a novel method involving co-precipitation of nickel dimethyl glyoxime and ceric hydroxide from a solution of ammonium cerium nitrate and nickel nitrate followed by calcination of the dried powder in air at 500 °C for 2 hours. The XRD analysis confirmed a cubic fluorite structure for the synthesized $CeNi_{0.5}O_y$ nanoparticles and a crystallite size of 4-5 nm. For reduction, the $CeNi_{0.5}O_y$ were mixed with oxalic acid and heated to 400 ºC in a closed stainless steel vessel. Thermal decomposition of oxalic creates a reducing atmosphere. In the XRD spectra of the reduced samples, the shift of diffraction lines towards lower angles confirming the lattice expansion by the formation of anionic vacancies and the insertion of hydrogen into the lattice of $CeNi_{0.5}O_y$ during reduction. A mechanism has been proposed for the insertion of H_2 into the fluorite lattice of $CeNi_{0.5}O_y$. The TPR with hydrogen results also reveals that $CeNi_{0.5}O_y$ is reduced by hydrogen and maximum intake of hydrogen occurs at 468.6 ºC. Raman spectrum was also used for the characterization. SEM image revealed the porous nature of the nanomaterial. The reduced and non-reduced samples of $CeNi_{0.5}O_y$ nanoparticles were also characterized using FT-IR analysis, UV-Vis analysis and Fluorescence spectroscopy. Spectra also supported the formation of $CeNi_{0.5}O_y$. The results presented in this paper demonstrate a facile approach for the synthesis and reduction of $CeNi_{0.5}O_y$ nanomaterial.

Acknowledgement

The authors P.J. Elsa and C.B. Jeena would like to thank Council of Scientific and Industrial Research (CSIR), India for JRF and P.G. & Research Department of Chemistry, Christ College (Autonomous), Irinjalakuda, affiliated to University of Calicut. P.P. Moly would like to thank UGC, India for the FDP support. K.J. Ambily would like to thank P.G. & Research Department of Chemistry, Christ College (Autonomous), Irinjalakuda, affiliated to University of Calicut.

References

[1] E. A. Berlouis et al., “Enhanced hydrogen storage in Ni / Ce composite oxides,” Phys. Chem. Chem. Phys., vol. 9, pp. 6032–6039, 2007.

[2] P. Jasinski, T. Suzuki, and H. U. Anderson, “Nanocrystalline undoped ceria oxygen sensor,” Sensors Actuators, B Chem., vol. 95, no. 1–3, pp. 73–77, 2003.

[3] Shobit Omar, “Doped Ceria for Solid Oxide Fuel

Cells."
[4] G. Wrobel, C. Lamonier, A. Bennani, A. D'Huysser, and A. Aboukaïs, "Effect of incorporation of copper or nickel on hydrogen storage in ceria. Mechanism of reduction," J. Chem. Soc., Faraday Trans., vol. 92, no. 11, pp. 2001–2009, 1996.
[5] K. Sohlberg, S. T. Pantelides, and S. J. Pennycook, "Interactions of Hydrogen with CeO 2," vol. 43, no. 11, pp. 6609–6611, 2008.
[6] M. L. Dos Santos et al., "Preparation and characterization of ceria nanospheres by microwave-hydrothermal method," Mater. Lett., vol. 62, pp. 4509–4511, 2008.
[7] M. A. Ebiad, D. R. A. El-hafiz, R. A. Elsalamony, and L. S. Mohamed, "Ni supported high surface area CeO 2 – ZrO 2 catalysts for hydrogen production from ethanol steam reforming," RSC Adv., vol. 2, pp. 8145–8156, 2012.
[8] C. L. Jalowiecki-Duhamel, A. Ponchel, "Storage of reactive hydrogen species in CeMxOy (M=Cu, Ni; 0<x<1)mixed oxides," Int. J. Hydrogen Energy, vol. 24, pp. 1083–1092, 1999.
[9] C. Lamonier, A. Ponchel, and A. D. Huysser, "Studies of the cerium-metal-oxygen-hydrogen system (metal=Cu, Ni)," Catal. Today, vol. 50, pp. 247–259, 1999.
[10] W. Shan, M. Luo, P. Ying, W. Shen, and C. Li, "Reduction property and catalytic activity of Ce1−XNiXO2 mixed oxide catalysts for CH 4 oxidation," Appl. Catal. A Gen., vol. 246, pp. 1–9, 2003.
[11] Y. H. Liu, J. C. Zuo, X. F. Ren, and L. Yong, "Synthesis and character of cerium oxide (CeO2) nanoparticles by the precipitation method," METALURGIJA, vol. 53, no. 4, pp. 463–465, 2014.
[12] A. P. Jalowiecki-Duhamel, J. Carpentier, "Hydrogen storage in cerium nickel and zirconium (or aluminium) mixed oxides .," in WHEC 16 / 13-16 June 2006 – Lyon France Hydrogen, 2006.
[13] P. Song, X. Zhang, M. Sun, X. Cui, and Y. Lin, "Synthesis of graphene nanosheets via oxalic acid-induced chemical reduction of exfoliated graphite oxide," RSC Adv., vol. 2, no. 3, p. 1168, 2012.
[14] A. Ponchel, A. D'huysser, C. Lamonier, and L. Jalowiecki-duhamel, "CeNi O and CeAl Ni O solids studied by electron microscopy," Phys Chem Chem Phys, vol. 2, pp. 303–312, 2000.
[15] T. Kakumoto and A. Imamura, "Unimolecular Decomposition of Oxalic Acid," J. Phys. Chem., no. 3, pp. 2366–2371, 1987.
[16] M. Daturi, E. Finocchio, C. Binet, J. C. Lavalley, F. Fally, and V. Perrichon, "Study of Bulk and Surface Reduction by Hydrogen of Ce x Zr 1 - x O 2 Mixed Oxides Followed by FTIR Spectroscopy and Magnetic Balance," J. Phys. Chem. B, vol. 103, pp. 4884–4891, 1999.
[17] S. Vivek, P. Arunkumar, and K. S. Babu, "In situ generated nickel on cerium oxide nanoparticle for efficient catalytic reduction of 4- nitrophenol.," RSC Adv., vol. 6, pp. 45947–45956, 2016.
[18] M. A. R. R. Radhakrishnan, "Microstructural properties and antibacterial activity of Ce doped NiO through chemical method," SN Appl. Sci., vol. 1, no. 3, pp. 1–9, 2019.
[19] C. Sun, H. Li, H. Zhang, Z. Wang, and L. Chen, "Controlled synthesis of CeO 2 nanorods by a solvothermal method," Nanotechnology, vol. 16, no. 9, pp. 1454–1463, 2005.
[20] P. Tamizhdurai, S. Sakthinathan, S. M. Chen, K. Shanthi, S. Sivasanker, and P. Sangeetha, "Environmentally friendly synthesis of CeO2 nanoparticles for the catalytic oxidation of benzyl alcohol to benzaldehyde and selective detection of nitrite," Sci. Rep., vol. 7, no. 1, pp. 1–13, 2017.
[21] M. R. M. Signorelli, R. C. Rabelo-neto, and L. V Mattos, "Nickel / Doped Ceria Solid Oxide Fuel Cell Anodes for Dry Reforming of Methane," vol. 25, no. 12, pp. 2356–2363, 2014.
[22] W. Fang et al., "Room Temperature Hydrogen Production from Ethanol over CeNi X H Z O Y Nano-Oxyhydride Catalysts," ChemCatChem, vol. 5, no. 8, pp. 2207–2216, 2013.
[23] L. He et al., "Cerium-oxide-modified nickel as a non-noble metal catalyst for selective decomposition of hydrous hydrazine to hydrogen," ACS Catal., vol. 5, no. 3, pp. 1623–1628, 2015.